PHYSICAL REVIEW A VOLUME 41, NUMBER 1 1 JANUARY 1990

Radiative distortion of the hydrogen atom in superintense, high-frequency fields of linear polarization

M. Pont, N. R. Walet,* and M. Gavrila
FOM-Institute for Atomic and Molecular Physics, Kruislaan 407,
1098 SJ Amsterdam, The Netherlands

(Received 24 February 1989)

We study the structure of the hydrogen atom when placed in a high-frequency, superintense laser field, within the framework of a nonperturbative theory recently developed for this purpose. The theory predicts that in the high-frequency limit the atom is stable against decay by multiphoton ionization, and that its structure is determined by a time-independent Schrödinger equation containing a "dressed" Coulomb potential. The laser frequency ω and the intensity I enter only combined in the parameter $\alpha_0 = I^{1/2}\omega^{-2}$ a.u. We first analyze the symmetry of the eigenvalue problem for the case of linear polarization under consideration and adopt an appropriate classification scheme for the levels. The small-α_0 limit of the levels is obtained analytically. In the large-α_0 limit scaling laws are derived for the α_0 dependence of the eigenvalues and eigenfunctions. At finite α_0 we have carried out a very accurate numerical computation over an extended range of α_0 values $(0 \le \alpha_0 \le 200$ a.u.) for a number of symmetry manifolds, by diagonalization of the Hamiltonian in a Gaussian basis. The correlation diagrams relating the small- and large-α_0 limits exhibit several avoided crossings. The binding energies show an overall decrease with α_0, in some cases preceded by an increase through a maximum. For the ground state this decrease is quite steep. The extreme distortion of the atomic structure accompanying it is studied. It is shown that, with increasing α_0, the (oscillating) electronic cloud undergoes radiative stretching, which eventually culminates at large α_0 in its splitting into two parts (dichotomy). The consequences of our findings for the experimental energy spectrum of the ejected electrons are considered.

I. INTRODUCTION

An atom placed in a radiation field undergoes distortion, while ionizing by absorption of one or several photons. The distortion sets in gradually with the intensity of the radiation, but becomes important only when this attains rather high values. For a hydrogen atom in the ground state, this will happen around the "atomic unit" of intensity $I_0 = 3.51 \times 10^{16}$ W/cm^2, at which, by definition, the amplitude of the oscillating electric field equals the electrostatic field created by the proton on the first Bohr orbit. Present-day lasers can already generate such superintense fields, in the form of radiation pulses of picosecond duration or less. Intensities orders of magnitude higher are expected in the near future.[1] It is the atomic behavior in this regime of intensities that we are interested in.

Under these circumstances it becomes insufficient to apply the standard perturbation theory formulas to lowest nonvanishing order, because higher-order terms in the perturbation expansion become comparable to the lower-order ones and should therefore be included, let aside the uncertainties concerning the convergence of the summation. The alternative is to devise direct, nonperturbative approaches for solving the Schrödinger equation of the atom in an intense field.

One such theory, valid at sufficiently high frequencies, was presented a few years ago by Gavrila and Kaminski.[2,3] It has been applied so far to the scattering and ionization of one-electron systems. The case of potential scattering was treated first.[4] This was followed by the study of the structure of atomic hydrogen, in linearly[5,6] and circularly polarized fields.[7] An exploratory calculation[5] for *linear polarization*, the only case we shall be interested in in the following, has revealed a striking overall decrease with intensity of the binding energies of the (nondecaying) states in the high-frequency limit.[8] In order to fully understand the accompanying distortion of the hydrogen atom, we have initiated a very accurate structure computation. For the ground state this has already revealed[6] an unprecedented stretching of the oscillating electron charge density along the direction of the electric field, culminating in its splitting into two parts (*dichotomy*). This occurs at intensities within experimental reach.

In the following we present a full account of our results on the structure of the hydrogen atom, which includes the ground state and a number of lower-lying excited states. The layout is as follows. In Sec. II we briefly recall the basic equations and underlying assumptions of the high-frequency theory we are using. In the high-frequency limit one needs solve just one eigenvalue equation, which contains a radiation modified potential depending on the frequency and intensity of the field through a parameter α_0. In Sec. III we discuss the symmetry of the eigenvalue problem. This will allow us to develop correlation diagrams for the eigenvalues $E(\alpha_0)$ when α_0 is varied from 0 (unperturbed atom) to very large values (dichotomized atom). In Sec. IV it is shown that the small-α_0 dependence of the levels can be ob-

© 1990 The American Physical Society

tained analytically in agreement with the result of standard lowest-order perturbation theory (at high frequencies). Section V studies analytically the large-α_0 limit, in which atomic dichotomy occurs. Scaling laws for the energy levels and wave functions are deduced for this limit. The numerical methods are presented in Sec. VI. The calculation was carried out by diagonalization of the Hamiltonian in a large Gaussian basis. The results are given and discussed in Sec. VII. There we first present the α_0 dependence of the lowest-lying eigenvalues for a number of symmetry classes, and their correlation diagrams. Also illustrated is the radiative stretching of the eigenfunctions, culminating at large α_0 in full dichotomy. We finally discuss the experimental implications of our results. Among others, it follows that the energy spectrum of the ejected electrons (as they are leaving the atom) is displaced towards higher energies.

II. BASIC FORMALISM

The starting point of the high-frequency theory[2,3] is the "space-translated" version of the semiclassical Schrödinger equation for a particle moving under the combined forces of a potential $V(\mathbf{r})$ and a radiation field. This was derived by Kramers[9] (see also Pauli and Fierz[10]) in the general context of quantum electrodynamics, and independently by Henneberger[11] for laser-atom interactions. It assumes that the radiation field can be described by its dipole approximation in the physically important region of space; we denote the corresponding vector potential by $\mathbf{A}(t)$. By applying the time-dependent translation $\mathbf{r}\rightarrow\mathbf{r}+\boldsymbol{\alpha}(t)$ with

$$\boldsymbol{\alpha}(t)=-\frac{e}{mc}\int_0^t \mathbf{A}(t')dt' \tag{1}$$

to the one-electron Schrödinger equation in the momentum gauge (for the laboratory frame of reference), the space-translated version emerges

$$\left[\frac{1}{2m}\mathbf{P}^2+V(\mathbf{r}+\boldsymbol{\alpha}(t))\right]\psi=i\hbar\frac{\partial\psi}{\partial t} . \tag{2}$$

Note that in passing from the momentum gauge form of the Schrödinger equation to Eq. (2), we have removed the term $e^2\mathbf{A}^2(t)/2mc^2$ by a phase-factor transformation.[12] We are using in this section the Gaussian system of units.

As easily seen, Eq. (1) represents the field-driven part of the motion of a classical free electron. Thus, Eq. (2) characterizes the dynamics of our problem in a moving frame of reference which follows the field-driven motion of the classical electron (i.e., in which it moves with constant velocity). This we shall call the "Kramers reference frame." In it the center of force (the proton) has a motion represented by $-\boldsymbol{\alpha}(t)$, as apparent also in Eq. (2).

From now on we shall assume that the radiation field can be represented by a *monochromatic plane wave* of frequency ω (i.e., with constant amplitude in space and time). By so doing we confine ourselves to a regime of stationary atomic distortion and decay.

For *linear polarization,* the vector potential of the field in the laboratory frame can be written as $\mathbf{A}(t)=a\mathbf{e}\cos\omega t$, where $\mathbf{e}$ is the real unit vector of the polarization. Equation (1) then gives

$$\begin{aligned}\boldsymbol{\alpha}(t)&=\alpha_0\mathbf{e}\sin\omega t ,\\ \alpha_0&=-(ea/mc\omega) ,\end{aligned} \tag{3}$$

which describes the quiver motion of a classical electron. In atomic units (Bohr radii) the quiver amplitude α_0 becomes

$$\alpha_0=I^{1/2}\omega^{-2} , \tag{4}$$

where I is the time-averaged beam intensity in atomic units, $I_0=3.51\times10^{16}$ W/cm^2, and the photon energy is given in hartrees (2 Ry).

By inserting Eq. (3) into Eq. (2) one gets a differential equation with periodic coefficients, which can be handled according to the Floquet method.[2,3] This leads to a system of coupled differential equations in coordinate space for the Floquet components of the wave function ψ, containing a (in general, complex) quasienergy parameter E. The system has to be supplemented by an appropriate boundary condition to describe steady decay by multiphoton ionization of an initial state in the field. An iterative method of solution was devised, proceeding essentially in inverse powers of ω. To lowest order in the iteration, i.e., in the *high-frequency limit,* the set of coupled equations reduces to a single one,

$$\left[\frac{1}{2m}\mathbf{P}^2+V_0(\alpha_0,\mathbf{r})\right]\psi_0=E\psi_0 . \tag{5}$$

This has the form of a time-independent Schrödinger equation for the zeroth Floquet component ψ_0, the only one in the expansion of ψ to survive in this limit. Thus

$$\psi(\mathbf{r},t)\cong\psi_0(\mathbf{r})\exp(-iEt/\hbar) . \tag{6}$$

Equation (5) contains the "dressed potential" $V_0(\alpha_0,\mathbf{r})$, which is the time average over a period of the oscillating $V(\mathbf{r}+\boldsymbol{\alpha}(t))$

$$V_0(\alpha_0,\mathbf{r})=\frac{1}{2\pi}\int_0^{2\pi}V(\mathbf{r}+\alpha_0\mathbf{e}\sin\zeta)d\zeta . \tag{7}$$

The result has a simple intuitive meaning: in the high-frequency limit the electron is not capable of "feeling" the rapidly oscillating potential $V(\mathbf{r}+\boldsymbol{\alpha}(t))$, but only its time average V_0. In the Coulomb case $V(r)=-e^2/r$, Eq. (7) can also be looked upon as the electrostatic potential created by a linear (inhomogeneous) distribution of charges extending from $-\alpha_0$ to $+\alpha_0$ along the line of oscillation of direction $\mathbf{e}$ passing through the center of force [see Eq. (2) of Ref. 5].

The dressed Coulomb potential can be expressed as

$$\begin{aligned}V_0(\alpha_0,\mathbf{r})=&-(2e^2/\pi)(r_+r_-)^{-1/2}\\ &\times K(2^{-1/2}(1-\hat{\mathbf{r}}_+\cdot\hat{\mathbf{r}}_-)^{1/2}) ,\end{aligned} \tag{8}$$

where $\mathbf{r}_\pm=\mathbf{r}\pm\alpha_0\mathbf{e}$ [the origin of the coordinates is kept at the center of $V(r)$] and K is the complete elliptic integral of the first kind. V_0 has $r^{-1/2}$ singularities at the end points of the charge distribution $\pm\alpha_0\mathbf{e}$, and a logarithmic singularity along the segment between them [due to the behavior of $K(x)$ for $x\rightarrow1$]. A graphical representation of V_0 was given in Fig. 1 of Ref. 2.

It is apparent from Eq. (5) that, in the high-frequency limit, ω and I enter the theory only through the parameter α_0 [Eqs. (3) and (4)] contained in V_0. Whereas in general the quasienergies E are complex, Eq. (5) has obviously real eigenvalues, indicating that in the high-frequency *limit* the atom is stable ("high-frequency stabilization"), i.e., cannot decay by multiphoton ionization. On the other hand, it may be strongly distorted if the potential V_0 differs substantially from V (case of large α_0). Ionization becomes possible in the *second order* of the iteration, which yields an imaginary part to E,[13] and, at the same time, expressions for the n-photon ionization rates in terms of the solutions of Eq. (5). It is argued elsewhere[2,14] that the *frequency condition* under which the iteration procedure should converge (in some pragmatic sense) is

$$\hbar\omega \gg |E_0^m(\alpha_0)| \ , \tag{9}$$

where $E_0^m(\alpha_0)$ represents the lowest eigenvalue of the manifold having the same magnetic quantum number m as the initial state.[15] Note that the condition refers to the *atom in the field,* characterized by a given value of α_0. There are no restrictions on α_0 (except for being kept finite); i.e., the theory applies as well for $\alpha_0 \ll 1$, which is the realm of perturbation theory,[14] as for $\alpha_0 \gtrsim 1$, where the theory is nonperturbative. It is in this latter case that we shall be primarily interested.[16]

As evident from Eq. (4), the value of α_0 depends more sensitively on ω than on I. Very high values of ω would more readily satisfy the validity criterion of Eq. (9), but on the other hand would lead to small values of α_0, related to perturbation theory. In order to attain interesting, large values of α_0, it is desirable to keep ω as low as possible, compatible with Eq. (9), so that the intensity need not be prohibitively high. [The validity condition Eq. (9) will be discussed in Sec. VII A below.]

The solution ψ of Eq. (2) and its approximate form for the high-frequency limit Eq. (5) pertain to the Kramers reference frame. In the laboratory frame, the solution of the Schrödinger equation in the momentum gauge corresponding to Eq. (6) is[12,17]

$$\psi_L(\mathbf{r},t) \cong \psi_0(\mathbf{r}-\boldsymbol{\alpha}(t))\exp[(-it/\hbar)(E+e^2a^2/4mc^2)] \ . \tag{10}$$

ψ_L and the electronic charge density $|\psi_L|^2$ oscillate without loss of normalization, like a free classical electron.[18] From Eq. (10) it is apparent that the energy spectrum (including the continuum threshold) for the Schrödinger equation in the laboratory frame is shifted with respect to that given by Eq. (5) by the constant $e^2a^2/4mc^2$.

Equation (5) was obtained earlier via other methods by Henneberger[11] and Gersten and Mittleman[19] (see also Mittleman[20]), and solved for the ground-state energy in some cases.[21] Gersten and Mittleman were the first to realize its high-frequency character.[22] From now on, in the following sections, we shall be using *atomic units* ($|e|=\hbar=m=1$).

III. SYMMETRY MANIFOLDS

For any spherically symmetric potential $V(r)$, the dressed potential, Eq. (7), obviously has axial symmetry around the axis of $\mathbf{e}$, and is an even function with respect to its center. This reduction of the spherical symmetry implies that now only the projection of the angular momentum on the $\mathbf{e}$ axis (associated quantum number m) and the parity (quantum number P) are conserved quantities. In fact, as can be easily seen, the eigenvalues depend on $|m|$, rather than on m, which implies a twofold degeneracy for $m \neq 0$. The symmetry of the problem ($D_{\infty h}$) therefore suggests a classification scheme for the states similar to that for diatomic molecules (although the form of the potential is quite different in the two cases). Thus we will designate the states with $|m|=0,1,2,\ldots$ by $\sigma,\pi,\delta,\ldots$, respectively, and even or odd (gerade or ungerade) parity by $P=0$ or 1. In order to distinguish a particular state within a manifold with given $|m|$ and P, we will label it by the quantum numbers (n,l) of the unperturbed state it is connected to continuously in the field-free limit ($\alpha_0=0$), see Sec. IV. The eigenfunctions will therefore be denoted by $\phi_{(nl)m}(\mathbf{r})$; their parity is necessarily that of l.

One may inquire if for the dressed Coulomb potential there are no extra constants of the motion besides those mentioned. This may occur in the form of "dynamical" (i.e., potential dependent) quantities. The occurrence of the latter appears to be linked to the separability of the Schrödinger equation in some special system of coordinates. Whereas for two Coulomb centers (i.e., the $H_2{}^+$ problem with fixed nuclei) this is indeed the case,[23] it does not happen for more than two centers.[24] The dressed Coulomb potential is generated by an infinite (continuous) distribution of centers. It is therefore very unlikely that symmetries, other than the ones mentioned, be present.

It will be shown in Secs. IV and V that at small and large α_0 the eigenvalue problem can be solved separately, in part analytically. This enables the drawing of "correlation diagrams" for the eigenvalue curves $E(\alpha_0)$, which connect the small- and large-α_0 eigenvalues lying within the same symmetry manifold. If all symmetries of the problem are fully accounted for, the von Neumann–Wigner[25] "noncrossing rule" should be satisfied. This leads in general to "avoided crossings" of the eigenvalue curves at places where in an approximate calculation with a Hamiltonian of higher symmetry the curves would have crossed. We have computed the $E(\alpha_0)$ curves for various low-lying levels, and shall discuss the outcome in Sec. VII. The fact that we have found no crossings within the $\{|m|,P\}$ manifolds supports the assumption that there exist no other conserved quantities.

Note that the high-lying states of each manifold are of the Rydberg type. This is due to the fact that for $r \gtrsim \alpha_0$ the dressed potential [Eqs. (7) and (8)] reduces to a Coulomb potential corrected by terms in $r^{-(2s+1)}$, with $s=1,2,\ldots$. The Rydberg character will be manifest only for those states whose wave function lies to a good extent in the Coulombic region of the potential, i.e., at radial distances well beyond α_0.

IV. SMALL-α_0 LIMIT

For small α_0 the dressed potential V_0 differs little from the original Coulomb potential V and one may apply (time-independent) perturbation theory with respect to α_0 in order to get the corrections to the Bohr levels. As a basis for the perturbation calculation we shall take the hydrogenic eigenfunctions

$$\langle \mathbf{r}|nlm\rangle=\psi_{nlm}(\mathbf{r})=R_{nl}(r)Y_{lm}(\hat{\mathbf{r}}) \ . \tag{11}$$

Because of the degeneracy of the unperturbed problem, we have to diagonalize the lowest order in α_0 form of the matrix of V_0-V in each subspace characterized by a given n. As the matrix elements of V_0 are diagonal with respect to m (m is a conserved quantum number), we need only calculate

$$W_{nlm,nl'm}=\langle nlm|V_0-V|nl'm\rangle \tag{12}$$

for all possible values of l,l'.

Defining the Fourier expansion of $V(r)=-1/r$ by

$$V(r)=\int \bar{V}(k)e^{i\mathbf{k}\cdot\mathbf{r}}d\mathbf{k} \ , \tag{13}$$

we have

$$\bar{V}(k)=-(2\pi^2k^2)^{-1} \ . \tag{14}$$

Inserting Eq. (13) into Eq. (7) one immediately finds the Fourier expansion of V_0 in the form

$$V_0(\alpha_0,\mathbf{r})=\frac{1}{2\pi}\int_\infty d\mathbf{k}\int_0^{2\pi}d\theta\,\bar{V}(k)e^{i\mathbf{k}\cdot(\mathbf{r}+\alpha_0\mathbf{e}\sin\theta)} \ . \tag{15}$$

For small values of α_0 one may expand $\exp(i\mathbf{k}\cdot\alpha_0\mathbf{e}\sin\theta)$ in powers of α_0. By keeping only the first three terms, the θ integral can easily be carried out to give

$$V_0(\alpha_0,\mathbf{r})-V(r)\cong\frac{\alpha_0^2}{4}\frac{1}{2\pi^2}\int_\infty\frac{1}{k^2}(\mathbf{e}\cdot\mathbf{k})^2e^{i\mathbf{k}\cdot\mathbf{r}}d\mathbf{k} \ . \tag{16}$$

The expansion in α_0 cannot be pushed further, because the coefficient of α_0^4 is divergent.

The right-hand side of Eq. (16) contains the generalized function

$$U(\mathbf{r})\equiv\frac{1}{2\pi^2}\int_\infty\frac{(\mathbf{e}\cdot\mathbf{k})^2}{k^2}e^{i\mathbf{k}\cdot\mathbf{r}}d\mathbf{k} \ , \tag{17}$$

which is singular at $\mathbf{r}=0$, and has a well-defined meaning only under an integral, as, for example, in Eq. (12). It was shown that Eq. (17) defines the distribution[26]

$$U(\mathbf{r})=\frac{4\pi}{3}\delta(\mathbf{r})-\left[\frac{2P_2(\mathbf{e}\cdot\hat{\mathbf{r}})}{r^3}\right]' \ , \tag{18}$$

where P_2 is a Legendre polynomial and $[\ ]'$ means that an integral containing the second term has to be evaluated first over the region outside a sphere of radius ϵ around the origin, and then let $\epsilon\to0$.[27]

By using Eq. (18), the calculation of Eq. (12) to lowest order in α_0 gives

$$W_{nlm,nl'm}=\alpha_0^2[\,+(\pi/3)\psi^*_{nlm}(0)\psi_{nl'm}(0) \\ -\tfrac{1}{2}\langle nl|r^{-3}|nl'\rangle\langle lm|P_2|l'm\rangle] \ . \tag{19}$$

The first term is nonzero only for $l=l'=0$, while the second term should be omitted in this case (see Ref. 27). The second term contains the radial matrix element $\langle nl|r^{-3}|nl'\rangle$ and the angular one $\langle lm|P_2|l'm\rangle$. As known, the latter vanishes unless l and l' have the same parity, and $|l-2|\le l'\le l+2$ (for $l,l'\ge0$). Consequently, only the radial matrix elements with $l'=l\ne0$ and $l'=l\pm2$ ($l\ge2$) are of interest. However, according to the Pasternack-Sternheimer selection rule[28]

$$\langle nl|r^{-3}|nl\pm2\rangle=0 \ . \tag{20}$$

This shows that the matrix W of Eq. (20) is diagonal with respect to l to order α_0^2. We find

$$W_{nlm,nl'm}=(\Delta E)_{nl|m|}\delta_{ll'} \ , \tag{21}$$

$$(\Delta E)_{nl|m|}=\alpha_0^2[(\pi/3)|\psi_{nlm}(0)|^2 \\ -\tfrac{1}{2}\overline{(r^{-3})}_{nl}\langle lm|P_2|lm\rangle] \ , \tag{22}$$

again with the understanding that the second term in Eq. (22) has to be omitted when $l=0$.[27] This result can also be derived by inserting the spherical harmonics expansion of V_0 in Eq. (12); one may thus show that the correction terms in Eq. (21) are of order α_0^3.[29]

With

$$|\psi_{nlm}(0)|^2=(\pi n^3)^{-1}\delta_{l0} \ , \tag{23}$$

$$\overline{(r^{-3})}_{nl}=[n^3l(l+1)(l+\tfrac{1}{2})]^{-1} \quad (l>0) \ , \tag{24}$$

$$\langle lm|P_2|lm\rangle=[l(l+1)-3m^2]/(2l-1)(2l+3) \ , \tag{25}$$

the value of the level displacement Eq. (22) ("dynamic Stark shift") becomes

$$(\Delta E)_{nl|m|}=\alpha_0^2\left[\frac{1}{3n^3}\delta_{l0}-\frac{l(l+1)-3m^2}{2n^3l(l+1)(l+\frac{1}{2})(2l-1)(2l+3)}(1-\delta_{l0})\right] \ . \tag{26}$$

This shows that for each $|m|$ value the first values of l up to some l_0 ($|m|\le l<l_0$) yield a $\Delta E>0$ (i.e., the perturbed levels are more weakly bound, whereas from l_0 onward, $\Delta E<0$. For $|m|=0,1,2$ the values of l_0 are 1,2,4, respectively.

Equations (12) and (21) indicate that at small α_0 the unperturbed hydrogenic eigenfunctions are still approximate eigenfunctions for our problem. This allows us then, by continuity with respect to α_0, to use the quantum numbers n,l to label the exact eigenstates at all α_0 (as mentioned in Sec. III).

Equation (26) represents the level shift of the Bohr levels when the nuclear charge is smeared along a small segment of length $2\alpha_0$, such that it generates the potential $V_0(\alpha_0,\mathbf{r})$ of Eq. (16). It can be easily shown that the dressed potential V_0 is equivalent to the one created by two Coulomb centers of charge $Z=\frac{1}{2}$ situated at a distance $R=2^{1/2}\alpha_0$. This is why Eq. (26) coincides with the generalization of a formula derived by Bethe for the $\mathrm{H_2}^+$ problem,[30] where two nuclei of charge Z are located at small internuclear separation R, and the aforementioned values are given to these parameters.

The level shift Eq. (26) was derived from our high-frequency limit theory at low intensities, to first order in $\alpha_0^2 \sim I$. As such, it should be identical to the result of *time-dependent* perturbation theory, to second order in $I^{1/2}$, at high frequencies. It can be indeed shown that this is the case.[14]

V. LARGE-α_0 LIMIT

We now analyze the large-α_0 features of the eigenvalue problem. We shall show that at sufficiently large α_0 the eigenfunction of any state splits into two practically nonoverlapping parts (atomic dichotomy). To this end we shall use here a consistency argument.[31] In the following we denote $\phi(\mathbf{r})=\psi_0(\mathbf{r})$.

Let us *assume* that for a given (large) value of α_0 the wave function $\phi(\mathbf{r})$ is concentrated around the two endpoints $\pm\alpha_0\mathbf{e}$ of the linear charge distribution generating V_0. Then $\phi(\mathbf{r})$ has significant values only in the regions of space characterized by $(r_-/\alpha_0)\ll 1$ and $(r_+/\alpha_0)\ll 1$. In these regions the potential V_0 reduces to [see Eq. (8)]

$$\begin{aligned} V_0(\alpha_0,\mathbf{r}) &\cong \tilde{V}_0(\alpha_0,\mathbf{r}_-) \quad \text{for } (r_-/\alpha_0)\ll 1\ , \\ V_0(\alpha_0,\mathbf{r}) &\cong \tilde{V}_0(\alpha_0,-\mathbf{r}_+) \quad \text{for } (r_+/\alpha_0)\ll 1\ , \end{aligned} \tag{27}$$

where

$$\tilde{V}_0(\alpha_0,\mathbf{r})=-(2/\pi)(2\alpha_0 r)^{-1/2}K(2^{-1/2}(1-\hat{\mathbf{r}}\cdot\mathbf{e})^{1/2})\ . \tag{28}$$

Designating by χ the angle between $\hat{\mathbf{r}}$ and $\mathbf{e}$, the "end-point potential," Eq. (28), becomes

$$\tilde{V}_0(\alpha_0,\mathbf{r})=-(2/\pi)(2\alpha_0 r)^{-1/2}K\left[\sin\frac{\chi}{2}\right]\ . \tag{29}$$

Note its overall $r^{-1/2}$ radial dependence and the nonspherical symmetry.[32]

According to our assumption, in the vicinity of the endpoint $+\alpha_0\mathbf{e}$ the potential V_0 can be replaced in the eigenvalue equation [Eq. (5)] by the simpler form $\tilde{V}_0(\alpha_0,\mathbf{r}_-)$. Introducing now the scaled variables $\boldsymbol{\xi}=\alpha_0^{-1/3}\mathbf{r}_-$, the equation becomes

$$\left[-\frac{1}{2}\Delta'-\frac{2^{1/2}}{\pi\xi^{1/2}}K\left[\sin\frac{\chi}{2}\right]\right]u=Wu\ , \tag{30}$$

where Δ' is the Laplacian with respect to the variables $\boldsymbol{\xi}$. Here u and W are related to ϕ and E by

$$u(\boldsymbol{\xi})=C\phi(\alpha_0^{1/3}\boldsymbol{\xi}+\alpha_0\mathbf{e}),\quad W=\alpha_0^{2/3}E\ , \tag{31}$$

where C is some constant depending on the normalization.

Equation (30) is independent of α_0. A bound-state (square integrable) eigensolution $u(\boldsymbol{\xi})$ essentially extends over a finite region in the space of the variable $\boldsymbol{\xi}$, and its asymptotic behavior for $\xi\to\infty$ is dominated by the factor $\exp[-(2|W|)^{1/2}\xi]$. This means that the corresponding $\phi(\mathbf{r})$ has significant values only in regions for which $(r_-/\alpha_0)=(\xi/\alpha_0^{2/3})\ll 1$, and is exponentially small elsewhere. A similar argument can be made for the region around the endpoint $-\alpha_0\mathbf{e}$, characterized by $(r_+/\alpha_0)=(\xi/\alpha_0^{2/3})\ll 1$.

This then confirms our starting assumption that indeed (to lowest order in $1/\alpha_0$) the dressed potential V_0 can support eigenfunctions which are concentrated around its end points $\pm\alpha_0\mathbf{e}$ and are vanishingly small in the rest of space. At sufficiently large α_0 the conclusion is valid for any bound state of V_0. This is what we mean by the *dichotomy* of the atom; for the ground state it was illustrated in Fig. 1 of Ref. 6.

Note that $\tilde{V}_0$ [Eq. (29)] still has axial symmetry although no more parity, and hence the eigenvalues W will depend only on $|m|$. To order the levels in each manifold $|m|$ we need an extra label j. We shall therefore use for the eigenvalues W the notation $W_{|m|j}$ (occasionally also $W_{\sigma j}$, $W_{\pi j}$, etc.). The eigenfunctions u depend however on m, and will be denoted u_{mj}.

From Eq. (31) we find the large-α_0 scaling laws

$$E_{|m|j}\cong\alpha_0^{-2/3}W_{|m|j}\ , \tag{32}$$

$$\phi_{mj}(\mathbf{r})\cong N_{mj}(\alpha_0)u_{mj}(\mp\alpha_0^{-1/3}\mathbf{r}_\pm)\ , \tag{33}$$

where $\mathbf{r}$ lies either in the vicinity of $+\alpha_0\mathbf{e}$ or $-\alpha_0\mathbf{e}$, respectively. $N_{mj}(\alpha_0)$ is a normalization constant for $\phi_{mj}(\mathbf{r})$, such that

$$\int |u_{mj}(\boldsymbol{\xi})|^2 d\boldsymbol{\xi}=1\ . \tag{34}$$

The values of the wave function $\phi_{mj}(\mathbf{r})$ throughout space are interrelated by the parity condition. As is easily seen, a ϕ_{mj}^P of well-defined parity P can be written in the vicinity of both end points $\pm\alpha_0\mathbf{e}$ in the form

$$\begin{aligned} \phi_{mj}^P(\alpha_0,\mathbf{r})\cong(2\alpha_0)^{-1/2}[\,&u_{mj}(\alpha_0^{-1/3}\mathbf{r}_-) \\ &+(-1)^P u_{mj}(-\alpha_0^{-1/3}\mathbf{r}_+)]\ . \end{aligned} \tag{35}$$

ϕ_{mj}^P is normalized to 1 because the two terms in Eq. (35) have a vanishing overlap integral, and we have imposed Eq. (34). The fact that Eq. (35) contains two linearly independent wave functions corresponding to the same eigenvalue $E_{|m|j}$ (or $W_{|m|j}$) shows that in the large-α_0 limit we are dealing with a gerade-ungerade degeneracy. At large but finite α_0 the energies $E_{|m|j}^P(\alpha_0)$ of the two states $\phi_{mj}^P(\alpha_0,\mathbf{r})$ will become different, and we thus get a gerade-ungerade level splitting. Let us consider this in the following.

We first note than an exact eigenfunction of the manifold $\{|m|,P\}$, like $\phi_{mj}^P(\mathbf{r})$, also has a definite symmetry with respect to reflections in the xy plane (i.e., a change of z into $-z$). Indeed, these reflections can be obtained by first performing reflections in the origin [which multiply the original ϕ_{mj}^P by $(-1)^P$], followed by rotations of an angle π around $\mathbf{e}$ [which multiply ϕ_{mj}^P by an extra $(-1)^m$]. Hence, by reflecting ϕ_{mj}^P in the xy plane its value gets multiplied by $(-1)^{P+m}$.

For our present purpose we shall call a function ϕ_{mj}^{P} which is invariant at reflections in the xy plane (i.e., for which $m+P$ is even) "symmetric," and "antisymmetric" otherwise (i.e., $m+P$ is odd). States like σ_g, π_u, and δ_g are "symmetric," whereas σ_u, π_g, and δ_u are "antisymmetric." We shall use the notation $\phi_{mj}^{S},\phi_{mj}^{A}$, respectively, and for the corresponding energies $E_{|m|j}^{S},E_{|m|j}^{A}$.

It will be shown in the Appendix that an *estimate* for the gerade-ungerade level splitting is given by

$$E_{|m|j}^{A}-E_{|m|j}^{S}\cong A_{|m|j}(\alpha_0)\exp[-2(2|W_{|m|j}|)^{1/2}\alpha_0^{2/3}] , \tag{36}$$

where $A_{|m|j}(\alpha_0)$ is some *positive,* relatively slowly varying function of α_0 at large α_0.[33]

Equation (36) shows that the gerade-ungerade splitting of the levels decreases exponentially at large α_0. It also shows that at given α_0 the splitting is larger for the higher-lying energy states (smaller $|W_{|m|j}|$), than for the lower ones. Moreover, since $A_{|m|j}(\alpha_0)$ is positive, the energy of the "symmetric" state lies below that of its "antisymmetric" counterpart. Consequently, for each pair of coupled states within the σ manifold we have $E_{\sigma j}^{u}>E_{\sigma j}^{g}$; within the π manifold $E_{\pi j}^{g}>E_{\pi j}^{u}$, and within the δ manifold $E_{\delta j}^{u}>E_{\delta j}^{g}$, etc.

From the coalescence of the gerade-ungerade energy curves and from the noncrossing rule within each manifold $\{|m|,P\}$ it follows that at given $|m|$, the lowest "symmetric" energy curve ($m+P$ even) pairs with the lowest "antisymmetric" curve ($m+P$ odd), the next "symmetric" curve with the next "antisymmetric" curve, and so on. One may inquire how the coalescent curves behave at small α_0, where they are labeled in terms of (n,l). It is not difficult to see that, considering the l quantum numbers available for each level of the unperturbed hydrogen atom, at small α_0 the ordering of the "symmetric-antisymmetric" pair is the same as at large α_0 (i.e., the "antisymmetric" curve is above the "symmetric" one), and that the n quantum number associated to the "antisymmetric" curve of a pair is one unit larger than that of the "symmetric" curve. The relation between the corresponding l quantum numbers is more intricate, and follows from the low-α_0 ordering of the levels established by Eq. (26).

Because of the underlying dichotomy, the large-α_0 limit is in a way similar to the separated atom limit of a homonuclear diatomic molecule. There are some basic differences, however. In the molecular case the two atoms can be physically separated, and the total energy tends to the finite sum of the atomic energies; in our limit complete separation cannot occur, and the energy tends to zero, see Eq. (32). Related to this is the fact that our endpoint wave functions $u_{mj}(\alpha_0^{-1/3}\mathbf{r})$ spread out as $\alpha_0^{1/3}$ when α_0 increases, whereas for the separated atoms there is no spread. Also, in the large-α_0 limit, because the endpoint potentials [Eqs. (27) and (28)] become stronger when approaching the segment connecting them, the electronic charge distributions around the endpoints will be slightly shifted towards each other.

At given large α_0, however, it is only the lower-lying energy states, for which the spatial extension of the endpoint function u is small with respect to α_0, which exhibit dichotomy. There will always exist highly excited states which do not have this behavior. These are the Rydberg-type states (see end of Sec. III), for which the wave function lies well outside the sphere of radius α_0. This indicates that at given α_0 the accuracy of Eqs. (32),(35), and (36) is expected to decrease as we pass from low-lying energy states to higher excited ones.

VI. NUMERICAL CALCULATION

The numerical solution of the eigenvalue problem Eq. (5) was carried out by diagonalization of the Hamiltonian matrix in an orthonormalized Gaussian basis, analogous to the procedure used in structure calculations for diatomic molecules (e.g., see Ref. 34). However, a number of specific features mentioned below distinguish our calculation from the latter.

Each symmetry manifold $\{|m|,P\}$ was considered separately. Since the potential V_0 is singular along the line of charges (see Sec. II), we have distributed the centers of the Gaussian basis functions $\chi_i(\mathbf{r})$ along this line, chosen as the z axis. (This is in contrast to the current procedure for diatomic molecules, where the Gaussians are centered on the two fixed nuclei.) Powers of x and y were included in the $\chi_i(\mathbf{r})$ to be able to reproduce the correct azimuthal angular dependence imposed by m. Finally the correct parity P was incorporated from the start. Thus a typical basis function has the form

$$\begin{aligned}\chi_i(\mathbf{r})=x^h y^k&\exp[-\gamma_i(x^2+y^2)]\\&\times\{(z-\beta_i)^{l_i}\exp[-\gamma_i(z-\beta_i)^2]\\&\quad+(-1)^{P+h+k+l_i}(z+\beta_i)^{l_i}\\&\quad\times\exp[-\gamma_i(z+\beta_i)^2]\}\ .\end{aligned} \tag{37}$$

The first step in the computation was to generate matrices in this basis: the symmetric overlap matrix $S_{ij}=\langle\chi_i|\chi_j\rangle$ (needed for the orthogonalization of the basis), and the Hamiltonian matrix $H_{ij}=\langle\chi_i|H|\chi_j\rangle$. The overlap matrix and the kinetic energy matrix $K_{ij}=\langle\chi_i|\frac{1}{2}P^2|\chi_j\rangle$ were calculated from known analytic expressions.[35] The computation of the matrix elements of V_0 is more cumbersome. For this we have used the integral representation of V_0 [Eq. (7)] in terms of the Coulomb potential of shifted origin

$$V(\mathbf{r}+\alpha_0\mathbf{e}\sin\zeta)=-|\mathbf{r}+\alpha_0\mathbf{e}\sin\zeta|^{-1} ,$$

since the matrix elements of the latter are known analytically.[35] We are then left with the one-dimensional integration over ζ; this was evaluated numerically using an adaptive quadrature.

Once we have calculated the Hamiltonian and the overlap matrices we can go over to an orthonormal basis, by the so-called "canonical" orthogonalization procedure.[36] Let U be the orthogonal matrix diagonalizing S

$$U^{\dagger}SU=s , \tag{38}$$

where s is the diagonal, real matrix containing the eigenvalues s_i ($s_i > 0$). It can be shown that the set of new functions $\chi_i' = \sum_n X_{ni}\chi_n$, where $X_{ni} = U_{ni}s_i^{-1/2}$ form an orthonormal basis. Hence the transformed matrix

$$H^\dagger = X^\dagger H X \ , \tag{39}$$

with matrix elements $H_{ij}^\dagger = \langle \chi_i' | H | \chi_j' \rangle$, can be diagonalized by standard procedures. Its eigenvectors can be expressed finally in terms of the original Gaussian basis functions χ_i. The advantage of the canonical orthogonalization procedure is that numerical difficulties arising from the occurrence of near-linear dependence in the Gaussian set (i.e., some of the eigenvalues s_i are close to zero) can be handled appropriately.[36]

The diagonalization of $H^\dagger$ poses no special difficulties. It leads to a number of lower-lying eigenvalues within each symmetry manifold, which are approximations (upper limits) to the true eigenvalues of the problem. How good they actually are depends on the choice made for the parameters β_i and γ_i contained in Eq. (37). To achieve convergence towards the best possible result is a more difficult task, and was done by varying the β_i, γ_i in the vicinity of an appropriately chosen set β_i^0, γ_i^0. (This is another feature contrasting our computation from the ones done for diatomic molecules.)

If all β_i, γ_i were allowed to vary simultaneously, we would end up with too large a number of parameters to be able to handle in the optimization problem. We have therefore adopted a procedure currently used in quantum chemistry calculations: if several basis functions of the same type [i.e., having common l_i, see Eq. (37)] are located at the same point (i.e., have a common β_i), we have chosen the exponents γ_i in a geometric progression with as ratio some number $M(l_i)$, such as to reduce the difficulties caused by near-linear dependence.[37] Since we have on the average some five functions of the same type on each center, this limits considerably the number of variables to be optimized. Eventually, only a few of the γ_i were allowed to vary *simultaneously*.

A nonlinear optimization of the energy was then performed by applying an automatic minimization routine. This calculates the gradient of the energy numerically in the vicinity of the chosen (β_i^0, γ_i^0) [the diagonalization problem is carried out anew for each value of the (β_i, γ_i)], and determines the direction of steepest descent. The procedure was iterated until convergence within the accuracy desired was achieved.

With all these restrictions, there still remains considerable freedom in choosing the basis functions Eq. (37), e.g, their total number, the number located on each center, and the values of the l_i. The adequacy of the choice made was checked by varying these features independently, and considering the effects on the energy and by inspection of the graphical representation (smoothness, stability) of the eigenfunctions.

We have investigated the four symmetry manifolds σ_g, σ_u, π_g, and π_u for values of α_0 ranging from 0 to 200.[16] Due to the fundamental importance of the hydrogen atom problem we have deemed it worthwhile to carry out a very accurate computation. Up to ten different centers and a maximal number of 100 basis functions were used to obtain the lowest lying level in each symmetry class to five significant figures for the σ states and to four figures for the π states. The accuracy for the excited states is somewhat lower.

VII. RESULTS AND DISCUSSION

A. Energy eigenvalues

The numerical results of our computation of the *eigenvalues*, grouped according to their symmetry manifold $\{|m|, P\}$, are given with all relevant digits in Tables I–IV. In order to facilitate the discussion we have also displayed them graphically in Fig. 1. [The solid curves $E(\alpha_0)$ in the figure were obtained by interpolation from the values in the tables; however, the curves were drawn only up to $\alpha_0 = 100$.]

TABLE I. Energy (in a.u.) of the lower-lying σ_g states of hydrogen as function of α_0 (in a.u.).

α_0	1*s*	2*s*	3*d*	3*s*	4*d*
0	−0.5	−0.125	−0.055 56	−0.055 56	−0.031 25
1	−0.402 37	−0.1119	−0.055 92	−0.051 58	−0.031 41
2	−0.319 74	−0.099 23	−0.057 20	−0.047 53	−0.031 95
3	−0.266 20	−0.090 20	−0.059 73	−0.044 52	−0.033 01
4	−0.229 17	−0.084 06	−0.063 25	−0.042 34	−0.034 29
5	−0.201 96	−0.080 99	−0.065 75	−0.040 93	−0.034 99
7	−0.164 43	−0.082 25	−0.062 83	−0.039 66	−0.033 94
10	−0.130 09	−0.082 21	−0.054 91	−0.038 39	−0.030 97
15	−0.098 136	−0.074 72	−0.045 36	−0.037 29	−0.027 50
20	−0.079 869	−0.066 26	−0.039 50	−0.037 94	−0.027 92
30	−0.059 703	−0.052 79	−0.038 56	−0.030 61	−0.025 43
40	−0.048 808	−0.043 46	−0.035 49	−0.025 59	−0.023 96
50	−0.041 883	−0.036 92	−0.032 14	−0.023 89	−0.022 06
60	−0.037 000	−0.032 18	−0.029 11	−0.023 14	−0.019 53
70	−0.033 335	−0.028 59	−0.026 44	−0.022 09	−0.017 57
85	−0.029 236	−0.024 74	−0.023 13	−0.020 34	−0.016 25
100	−0.026 182	−0.021 84	−0.020 23	−0.018 29	−0.015 22
200	−0.016 402	−0.013 53	−0.012 02	−0.011 12	−0.010 32

TABLE II. Energy (in a.u.) of the lower-lying σ_u states of hydrogen as function of α_0 (in a.u.).

α_0	$2p$	$3p$	$4p$	$4f$	$5f$
0	−0.125	−0.055 56	−0.031 25	−0.031 25	−0.02
1	−0.132 59	−0.057 65	−0.032 11	−0.031 30	−0.020 44
2	−0.145 87	−0.060 33	−0.033 09	−0.031 35	−0.020 90
3	−0.151 49	−0.060 46	−0.033 00	−0.031 71	−0.020 83
4	−0.149 86	−0.059 19	−0.032 39	−0.032 13	−0.020 51
5	−0.144 70	−0.057 51	−0.032 81	−0.031 60	−0.020 83
7	−0.131 52	−0.054 42	−0.035 08	−0.030 21	−0.022 01
10	−0.113 33	−0.052 60	−0.039 39	−0.028 92	−0.023 49
15	−0.091 428	−0.054 45	−0.038 03	−0.028 04	−0.022 57
20	−0.076 912	−0.053 20	−0.034 37	−0.027 71	−0.021 22
30	−0.059 125	−0.046 63	−0.030 14	−0.027 73	−0.021 33
40	−0.048 706	−0.040 33	−0.029 77	−0.024 14	−0.020 23
50	−0.041 860	−0.035 30	−0.028 25	−0.021 29	−0.019 59
60	−0.036 992	−0.031 36	−0.026 37	−0.019 78	−0.018 89
70	−0.033 326	−0.028 22	−0.024 46	−0.019 33	−0.017 23
85	−0.029 235	−0.024 64	−0.021 93	−0.018 36	−0.015 23
100	−0.026 179	−0.021 82	−0.018 96	−0.016 11	−0.013 65
200	−0.016 402	−0.013 53	−0.012 02	−0.011 16	−0.010 20

The $E(\alpha_0)$ curves belonging to the same manifold form a "correlation diagram" connecting the unperturbed atom ($\alpha_0=0$) eigenvalues to their fully dichotomized (large-α_0) counterparts. For all α_0 the correlation curves $E(\alpha_0)$ obviously have to satisfy the noncrossing rule (see Sec. III). Assuming ω to be fixed at some convenient value [large enough to satisfy Eq. (9)], the correlation curves $E(\alpha_0)$ then represent the dependence on the intensity (strictly speaking on $I^{1/2}$), as this varies from zero towards high values. The correlation diagrams of Fig. 1 resemble those encountered in the structure of diatomic molecules, the internuclear distance R corresponding to our α_0, and the united and separated atom limits to our unperturbed and dichotomized atom limits, respectively.

A general feature of the correlation curves $E(\alpha_0)$ is their global tendency to increase to zero at large α_0 values. In some cases this increase is monotonical [e.g., $(1s)\sigma_g,(2p)\pi_u$], in others it may be preceded by extrema [e.g., $(2s)\sigma_g,(3d)\sigma_g,(2p)\sigma_u$]. In the range $\alpha_0<40$ the increase is rather sharp for the lower states. It is quite dramatic for the ground state $(1s)\sigma_g$ (not fully represented in Fig. 1), whose binding energy drops at $\alpha_0=40$ to about $\frac{1}{10}$ its value at $\alpha_0=0$ ($|E(0)|=0.5$ a.u.). However, for the higher excited states, which start at $\alpha_0=0$ with an already small value of the binding energy, the increase is much slower and takes place over large α_0 intervals.

The *small*-α_0 part of the correlation curves can be compared with the analytic formula Eq. (26), derived from perturbation theory. This can indicate under which circumstances $E(\alpha_0)$ behaves at small α_0 as a decreasing

TABLE III. Energy (in a.u.) of the lower-lying π_g states of hydrogen as function of α_0 (in a.u.).

α_0	$3d$	$4d$	$5d$	$5g$
0	−0.055 56	−0.031 25	−0.02	−0.02
1	−0.055 72	−0.031 31	−0.020 03	−0.020 00
2	−0.056 12	−0.031 47	−0.020 11	−0.020 03
3	−0.056 53	−0.031 59	−0.020 16	−0.020 08
4	−0.056 74	−0.031 59	−0.020 15	−0.020 14
5	−0.056 63	−0.031 44	−0.020 25	−0.020 04
7	−0.055 52	−0.030 80	−0.020 49	−0.019 68
10	−0.052 52	−0.029 44	−0.021 06	−0.018 94
15	−0.046 80	−0.027 19	−0.022 18	−0.017 76
20	−0.041 74	−0.025 69	−0.022 49	−0.016 88
30	−0.034 19	−0.024 35	−0.020 33	−0.015 90
40	−0.029 02	−0.022 71	−0.018 00	−0.015 34
50	−0.025 33	−0.020 97	−0.016 18	−0.015 08
70	−0.020 37	−0.017 89	−0.014 38	−0.013 41
100	−0.016 04	−0.014 54	−0.012 67	−0.010 85
200	−0.010 04	−0.009 068	−0.008 524	−0.007 792

or an increasing function, see the discussion in Sec. IV. For very small α_0, Eq. (26) can be used as a check on the numerical computation. Figure 2 contains the comparison for the $(2p)\sigma_u$ and $(2p)\pi_u$ states. Equation (26) gives in these cases

$$\begin{aligned} E_{210} &= -(1/8)-(1/120)\alpha_0^2\,, \\ E_{211} &= -(1/8)+(1/240)\alpha_0^2\,, \end{aligned} \tag{40}$$

respectively, which correspond to the straight lines in Fig. 2. As apparent, the agreement with the numerical computation is excellent, well within the α_0^3 corrective terms to Eq. (26).

At *intermediate* α_0 a number of avoided crossings can be seen in Fig. 1. Some of them can be related to the curve crossings of our earlier calculation (Ref. 5) done in the "decoupled l-channel approximation." The explanation of these crossings is the following. The decoupled l-channel approximation was done with a spherically symmetric (albeit nonlocal) approximation for V_0, which also conserves, therefore, the l quantum number. Its symmetry manifolds are characterized by the quantum numbers $\{|m|,l\}$. When grouping the curves in manifolds of the type $\{|m|,P\}$ considered here, crossings will be obviously possible between curves of different l (see Figs. 2–4 of Ref. 5). The avoided crossings in Fig. 1 which are related to crossings of the earlier calculation were enclosed in dashed rectangles. The extent to which two $E(\alpha_0)$ curves

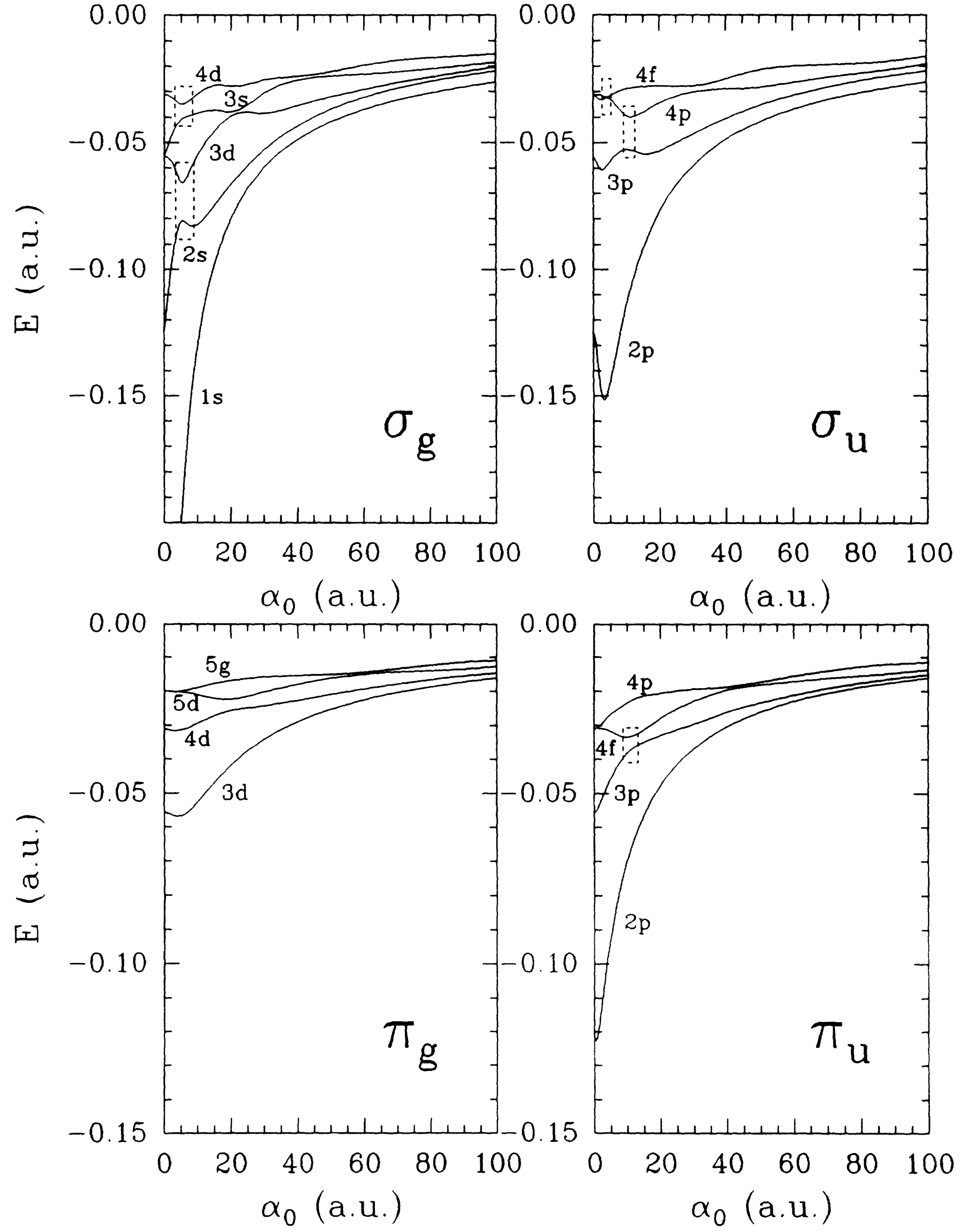

FIG. 1. The energies of the first eigenvalues of the σ_g, σ_u, π_g, and π_u manifolds as functions of α_0 (in a.u.). The dotted rectangles indicate avoided crossing corresponding to real crossings in the approximate calculation of Ref. 5.

TABLE IV. Energy (in a.u.) of the lower-lying π_u states of hydrogen as function of α_0 (in a.u.).

α_0	$2p$	$3p$	$4f$	$4p$
0	−0.125	−0.055 56	−0.031 25	−0.031 25
1	−0.1214	−0.054 51	−0.030 78	−0.030 71
2	−0.1141	−0.052 34	−0.030 85	−0.029 85
3	−0.1062	−0.049 97	−0.031 06	−0.028 80
4	−0.098 92	−0.047 70	−0.031 35	−0.027 74
5	−0.092 40	−0.045 61	−0.031 69	−0.026 73
7	−0.081 58	−0.042 04	−0.032 79	−0.025 38
10	−0.069 58	−0.038 01	−0.033 52	−0.023 43
15	−0.056 30	−0.034 85	−0.031 32	−0.021 34
20	−0.047 64	−0.033 49	−0.027 92	−0.020 61
30	−0.036 88	−0.029 66	−0.022 98	−0.019 38
40	−0.030 41	−0.026 22	−0.019 67	−0.018 77
50	−0.026 07	−0.023 41	−0.018 13	−0.017 24
70	−0.020 57	−0.019 19	−0.016 24	−0.014 02
100	−0.016 05	−0.015 07	−0.013 68	−0.011 48
200	−0.010 04	−0.009 064	−0.088 698	−0.008 169

repel each other at an avoided crossing characterizes the breakdown of the approximate calculation. This appears to be particularly severe within the rectangles connecting the σ_g states ($2s$) and ($3d$), and the σ_u states ($3p$) and ($4p$).[38]

The *large-*α_0 behavior of the correlation curves can be discussed in terms of the result of Eq. (32). Figure 3 contains the comparison for the states $(1s)\sigma_g$ and $(2s)\sigma_g$. Since the $W_{|m|j}$ entering Eq. (32) are not known, we shall assume this equation to be valid at $\alpha_0=200$ a.u., and, by inserting the numerical values of $E_{|m|j}(200)$ from Tables I–IV, we extract the corresponding $W_{|m|j}$. We find

$$\begin{aligned} W_{\sigma 1} &= -0.560\,94 \ , \\ W_{\sigma 2} &= -0.462\,72 \ . \end{aligned} \tag{41}$$

These we have used to draw the straight lines of slope $(-\frac{2}{3})$ representing Eq. (32) in the logarithmic plot of Fig. 3. For the ground state the agreement with the computed values at $\alpha_0=100$ and 85 is quite good and represents a check on both the computation and the asymptotic formula. In fact, the agreement extends to unexpectedly low values of α_0; for example at $\alpha_0=30$ the variance of the two calculations is of the order of 2%. For the $(2s)\sigma_g$ state the agreement sets in at larger values of α_0, reflecting the fact that dichotomy sets in later for excited states, as mentioned at the end of Sec. V.

The *gerade-ungerade splitting* occurring at large α_0 can be followed in Tables I–IV. In view of the results of Sec. V and of the noncrossing rule for the energy curves, the successive gerade and ungerade states of σ, π, δ, etc., type should coalesce in pairs at large α_0. Thus, for the σ type, the gerade states $1s$, $2s$, $3d$, etc., coalesce with the ungerade states $2p$, $3p$, $4p$, etc., respectively, and for the π type, the gerade states $3d$, $4d$, $5d$, etc., with the ungerade ones $2p$, $3p$, $4f$, etc., respectively. This is clearly borne out by the results of Tables I–IV. Furthermore, the "antisymmetric" state (in the sense of Sec. V) of coalescent pair has always higher energy than the "symmetric"

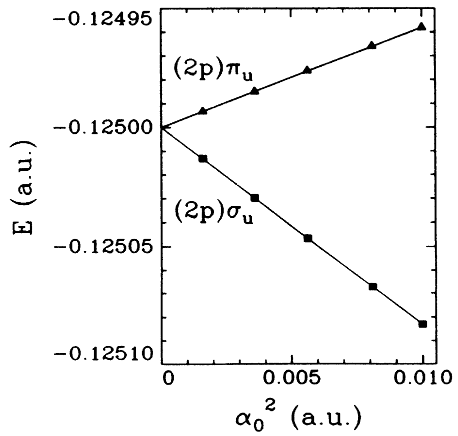

FIG. 2. The energies of the $(2p)\sigma_u$ and $(2p)\pi_u$ states at small α_0^2 (in a.u.). The straight lines through the points are the predictions of perturbation theory, see Eq. (40).

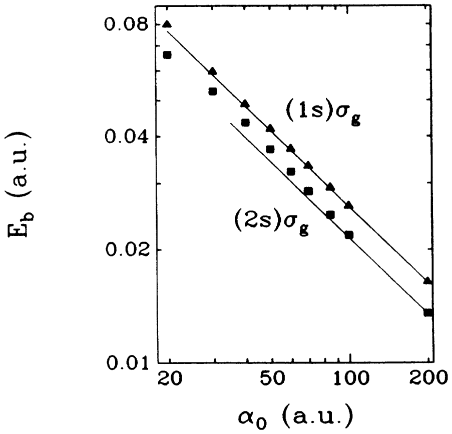

FIG. 3. The α_0 dependence of the binding energy $E_b=|E|$ of the ground state $(1s)\sigma_g$ and of $(2s)\sigma_g$ at large α_0, on a logarithmic scale (in a.u.). The drawn straight lines represent the asymptotic law of Eq. (32), with an approximate $W_{|m|j}$ given by Eq. (41).

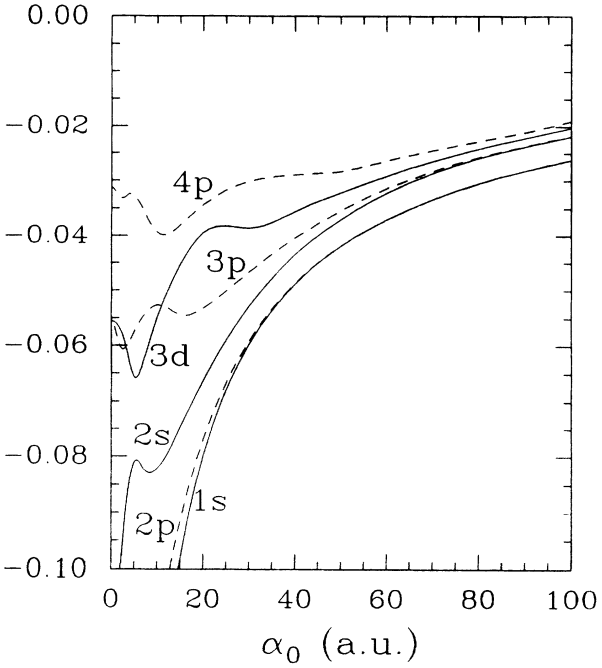

FIG. 4. Large-α_0 gerade-ungerade splitting of the eigenvalues for the lowest-lying three σ_g and σ_u states. The σ_g eigenvalues are fully drawn, the σ_u eigenvalues, dashed. The (n,l) labels of the states are as indicated. α_0 and E are in a.u.

state, in agreement with Eq. (36). These statements are illustrated in Fig. 4, which shows the pairwise coalescence of the first three gerade and ungerade σ states. Tables I–IV and Fig. 4 also show that the coalescence sets in at lower-α_0 values for the lower-energy states than for the higher ones, in agreement with what was said at the end of Sec. V.

At this point we would like to mention that the *convergence of the iteration procedure* of the high-frequency theory,[2,3] and, in particular, the validity of the high-frequency limit Eq. (5), are favorably influenced by the global decrease of the binding energies at large α_0. The exact Eq. (1) (or its equivalent Floquet version considered in Refs. 2 and 3) describes the structure of the atom in a field of given ω and α_0 (or ω and I). From the mathematical point of view, the high-frequency iteration will apply at any combination of ω and α_0 (or ω and I) such that the condition, Eq. (9), is well enough satisfied. The decrease of $|E_0(\alpha_0)|$ at large α_0 implies that at any given ω, if we choose I high enough that it will give a sufficiently large α_0, condition Eq. (9) will be satisfied for the ground state and the theory applies. In fact, the condition can be moderately well satisfied for already existing superintense lasers. With $\omega=5$ eV$=0.18$ a.u. and $I=10.5$ a.u. (corresponding to the upgraded KrF* excimer laser of Ref. 16), yielding $\alpha_0=100$, we have $\omega/|E_0(\alpha_0)|\cong 7$. The ionization of atoms under experimental circumstances, however, differs somewhat from the idealized situation described above; this will be discussed in Sec. VII C.

B. Energy eigenfunctions

In view of the φ dependence of the eigenfunctions $\phi_{(nl)m}(\mathbf{r})$, we may write

$$\phi_{(nl)m}(x,y,z)=e^{im\varphi}\zeta_{(nl)m}(r,\theta)\ . \tag{42a}$$

By setting $\varphi=0$, we find

$$\phi_{(nl)m}(x,0,z)=\zeta_{(nl)m}(r,\theta)\quad \text{for } x>0\ . \tag{42b}$$

Thus, knowledge of $\phi_{(nl)m}(x,0,z)$ is sufficient to determine $\phi_{(nl)m}(r)$ throughout space. Some of the $\phi_{(nl)m}(x,0,z)$ functions are represented in Figs. 5–7. The xz axes define the horizontal plane in Figs. 5 and 6, and the vertical axis gives the values of $\phi_{(nl)m}(x,0,z)$. In Fig. 7 the xz plane coincides with the plane of the figure, and the values of $\phi_{(nl)m}(x,0,z)$ are represented in terms of level lines.

We first consider the *distortion of the eigenfunctions* with increasing α_0. In Fig. 5 this is given for the states $(1s)\sigma_g$ and $(2p)\sigma_u$, the first coalescent gerade-ungerade pair of the σ type.

The case of the ground state wave function $(1s)\sigma_g$ was presented in more detail in Fig. 1 of Ref. 6. Note that the wave function does not change sign and maintains its value at reflections in the xz plane with respect to both the x or z axes. This follows from the fact that it has even parity $(P=0)$ and is "symmetric" at reflections in the xy plane $(P+m=0)$, see Sec. V.

From both Fig. 5 and Fig. 1 of Ref. 6 it is apparent that, with increasing α_0, the wave function undergoes *radiative stretching* in the z direction, following the elongation of the line of charges (length $2\alpha_0$) generating the dressed potential V_0 (for the shape of the latter see Fig. 1 of Ref. 2). However, as α_0 approaches 20 a saddle appears, and by $\alpha_0=30$ two pronounced maxima are formed around the end points $\pm\alpha_0\mathbf{e}$ of the line of charges. Beginning with $\alpha_0=50$, *dichotomy* sets in, and is complete by $\alpha_0=70$. While splitting, the wave function also becomes more diffuse around the endpoints (note the change of scale in the pictures of Fig. 5 for growing α_0). At large α_0 (e.g., $\alpha_0=200$), the ground-state wave function attains a truly Rydberg-state size (some $2\alpha_0=400$ a.u. linear extension).

In Fig. 5 we also show the parallel evolution of the $(2p)\sigma_u$ eigenfunction. This can take both positive and negative values, in such a way that it remains unchanged at reflections in the xz plane with respect to the z axis, and changes sign at reflections with respect to the x axis. Both properties follow from the fact that it has odd parity $(P=1)$ and is "antisymmetric" at reflections in the xy plane $(P+m=1)$, see Sec. V.

The $(2p)\sigma_u$ and the $(1s)\sigma_g$ wave functions are totally unrelated at lower α_0 values (e.g., $\alpha_0=10$). With increasing α_0 dichotomy sets in in both cases, and is complete by $\alpha_0=100$. By the time this happens the wave functions of the two states become related according to Eq. (35), illustrating the fact that we are dealing with a gerade-ungerade pair of states. The isolated peaks in the figures for $\alpha_0=100$ represent replicas of the ground-state

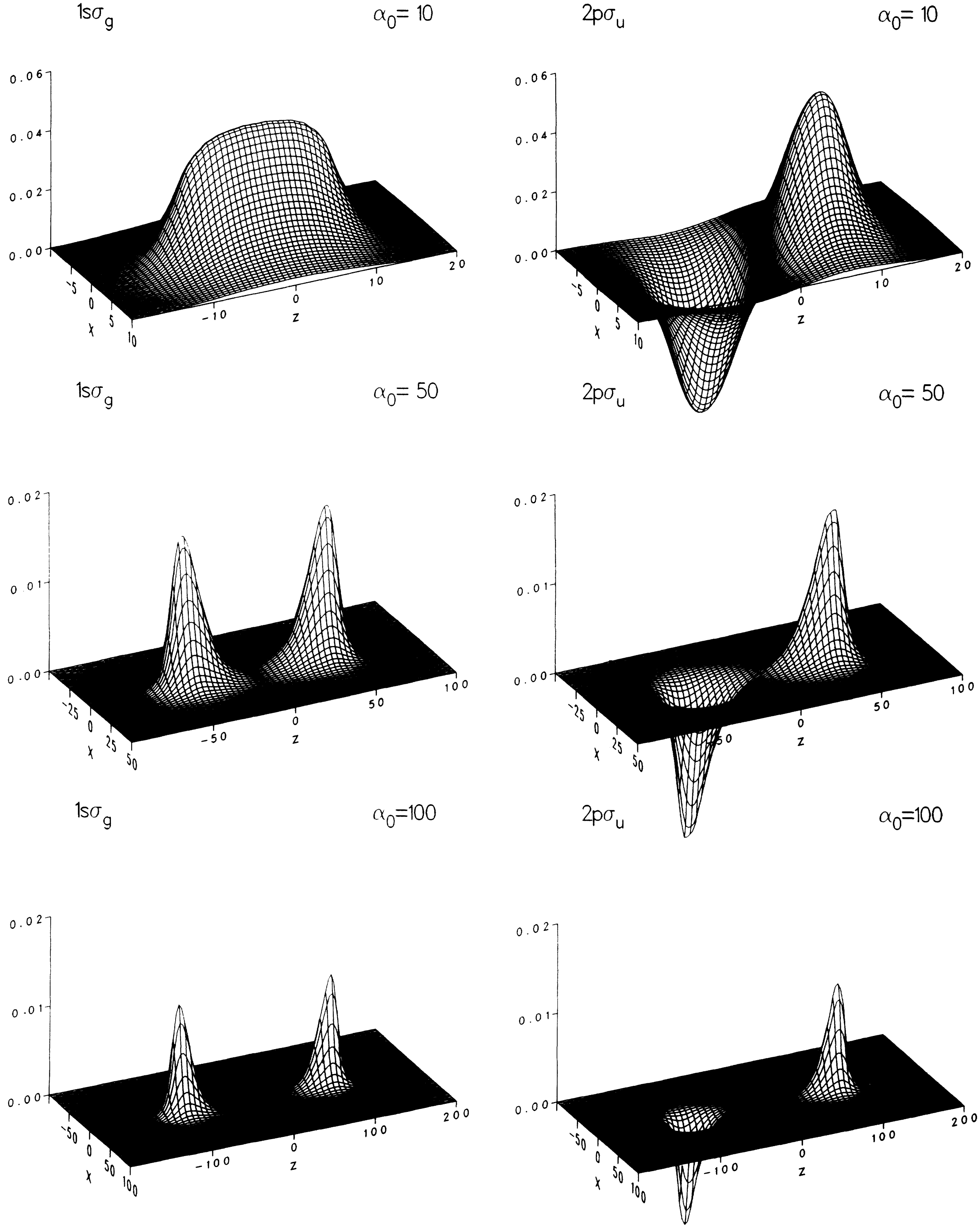

FIG. 5. The normalized eigenfunctions $\phi(x,0,z)$ of the $(1s)\sigma_g$ and $(2p)\sigma_u$ states in the Kramers frame of reference, for increasing α_0. The choice of the coordinate axes is defined in Sec. VII. The length unit is the Bohr radius a_0, and the unit for $\phi(x,0,z)$ is $a_0^{-3/2}$. There is a change of scale in the figures for the various α_0. Note how dichotomy begins to set in at about $\alpha_0=50$.

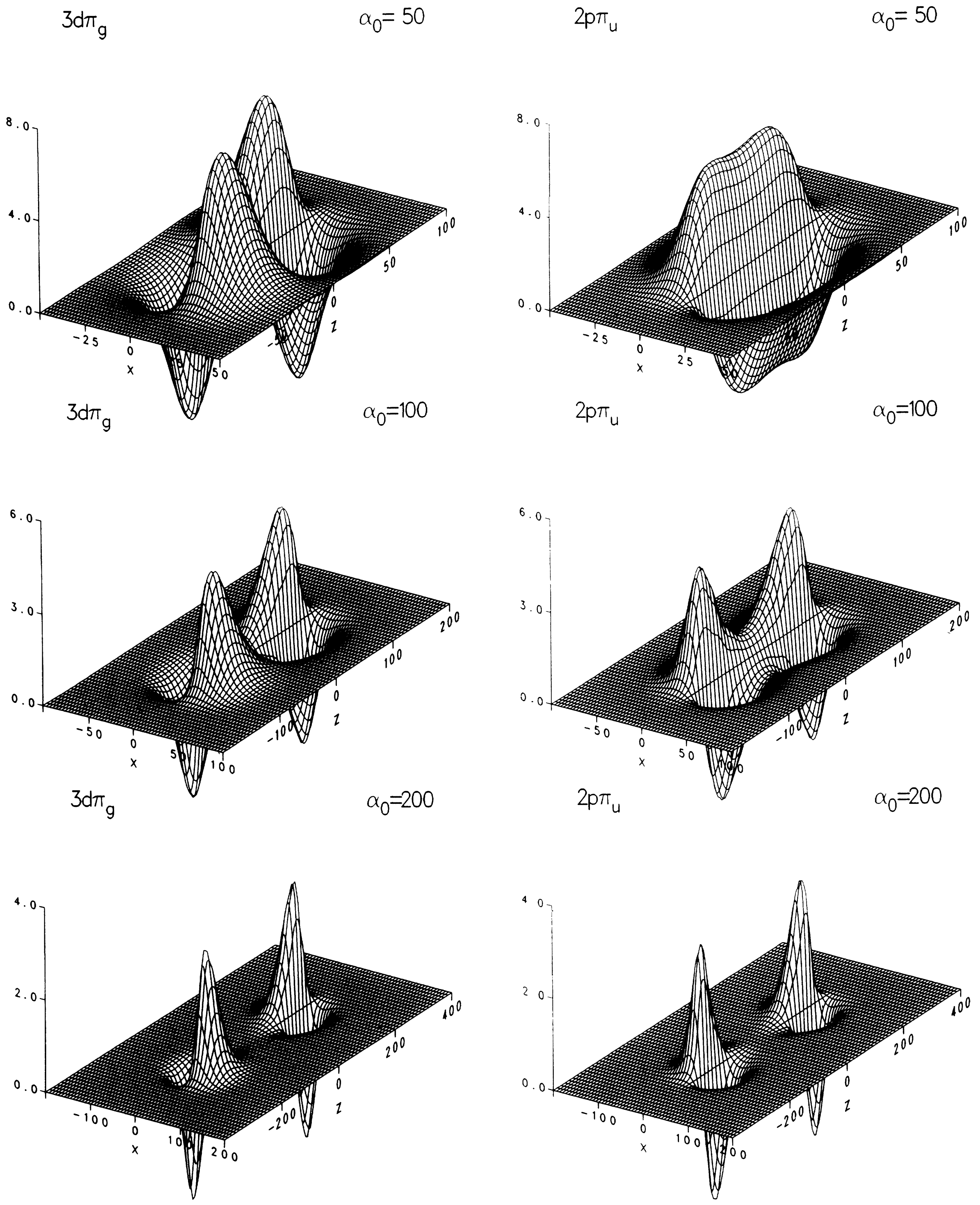

FIG. 6. The normalized eigenfunctions $\phi(x,0,z)$ of the $(3d)\pi_g$ and $(2p)\pi_u$ states in the Kramers frame of reference, for increasing α_0. The choice of the coordinate axes is defined in Sec. VII. α_0 is given in Bohr units a_0, whereas $\phi_0(x,0,z)$ is in units of $10^{-3}a_0^{-3/2}$. There is a change of scale in the figures for the various α_0. Note that dichotomy now sets in between $\alpha_0=100$ and 200.

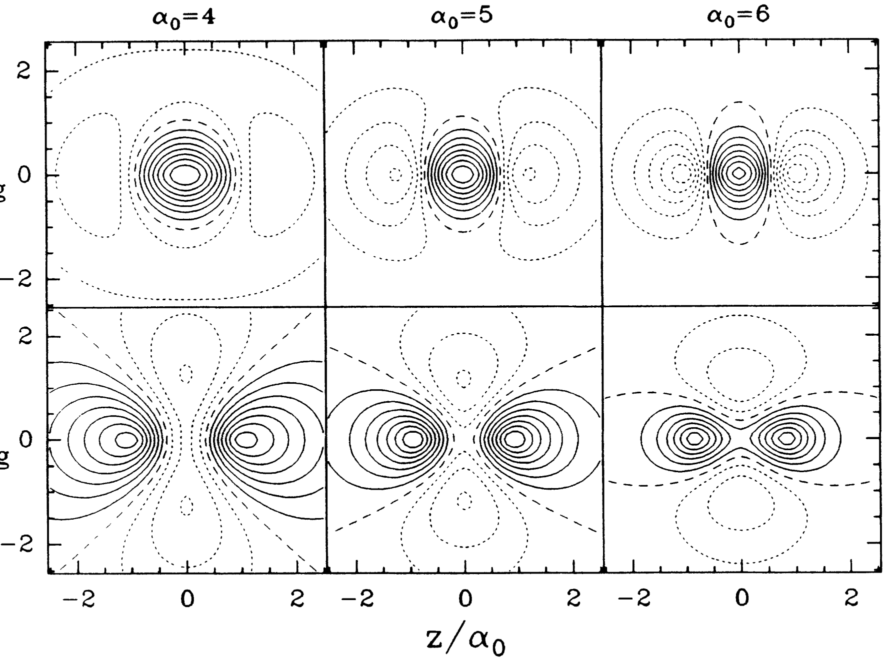

FIG. 7. Level plots of the eigenfunctions in the xz plane (defined as in Sec. VII) for the states $(2s)\sigma_g$ (upper three pictures) and $(3d)\sigma_g$ (lower three pictures), for α_0 in the vicinity of their avoided crossing, enclosed in the dotted rectangle of Fig. 1. The value of α_0 is the same for pictures on the same vertical, and is marked at the top ($\alpha_0=4,5,6$). The values of x and y are given in units of α_0. The distance of the level curves is 0.007 85 and 0.005 85 in the $(2s)\sigma_g$ and $(3d)\sigma_g$ cases, respectively. The positive level lines are drawn in full, the negative ones are dotted, and the zero level line is dashed.

eigenfunction of the end point potential Eq. (29) $[(2\alpha_0)^{-1/2}u_{\sigma 1}(\alpha_0^{-1/3}r)$ in the notation of Sec. V].

The evolution with α_0 of the first gerade-ungerade pair of the π type, $(3d)\pi_g$ and $(2p)\pi_u$, is given in Fig. 6. The $(3d)\pi_g$ wave function changes sign at reflections in the xz plane with respect to both x or z axes, whereas the $(2p)\pi_u$ wave function changes sign at reflections with respect to the z axis and retains its value at reflection with respect to the x axis. These properties follow from the corresponding P and $P+m$ values. Again, the shapes of the two eigenfunctions are totally unrelated at values of α_0 up to 50. It is apparent that dichotomy now sets in somewhere below $\alpha_0=200$, that is, at higher values than for the lower-lying states $(1s)\sigma_g$ and $(2p)\sigma_u$, in agreement with the remarks of Sec. V. However, by the time this happens, the two wave functions become again related by Eq. (35) and we are dealing essentially with replicas of the $u_{\pi 1}$ eigenfunction of the end-point potential Eq. (29).

Figure 7 illustrates the behavior of the eigenfunctions of the $(2s)\sigma_g$ and $(3d)\sigma_g$ states in the vicinity of the avoided crossing of their energy curves $E(\alpha_0)$ in the vicinity of $\alpha_0=5$, see the corresponding dashed rectangle in Fig. 1. Whereas at arbitrary values of α_0 changes in the form of the wave functions occur only over extended α_0 intervals, in the present case the wave functions change their shape rapidly within 1 a.u.

The $(2s)\sigma_g$ wave function evolves from the spherically symmetric hydrogenic wave function $R_{20}(r)$ at $\alpha_0=0$. A remnant of this behavior is still seen to survive at $\alpha_0=4$, e.g., the shape of the positive peak and the circular nodal line around it (represented by the dashed line in Fig. 7). As we pass the crossing point, however, deep minima appear on the z axis around $z=\pm\alpha_0$ (e.g., the case of $\alpha_0=6$), and the resemblance is lost. The $(3d)\sigma_g$ wave function, on the other hand, evolves from the hydrogenic wave function $R_{32}(r)P_2(\cos\theta)$ at $\alpha_0=0$, its angular dependence being characterized by the Legendre polynomial $P_2(\cos\theta)$ which vanishes for $\cos^2\theta=\frac{1}{3}$. A remnant of this behavior can still be seen at $\alpha_0=4$ (e.g., the quasistraight, although interrupted, nodal lines). Beyond $\alpha_0=5$ the shape is completely changed. Note that, because of the strong interaction of the energy curves $E(\alpha_0)$ around the avoided crossing, the shape of each of the wave functions below the value $\alpha_0=5$ is not transmitted to the other one above this value.

The stable, high-frequency limit eigenfunctions we have calculated and discussed pertain to the Kramers frame of reference. Their form in the laboratory frame can be obtained from Eq. (10).[18]

C. Experimental implications

The atomic structure we have been discussing so far pertains to the high-frequency *limit* of our theory. In fact, ω will be finite no matter how large. As mentioned in Sec. II, this can be taken into account by passing to the *second-order approximation* of the theory, which allows for atomic ionization. The latter manifests itself in the fact that the eigenvalues become complex, i.e., there is a shift and a broadening of the physical levels with respect to the values obtained here, and, at the same time, the wave functions lose their square integrability while acquiring diverging spherical waves. The latter yield the decay amplitudes for the various channels of multiphoton absorption. Nevertheless, the better the condition Eq. (9) is satisfied, the closer the exact results will be to the ones calculated here.

The energy spectrum of the photoelectrons depends on the binding energy $E_0(\alpha_0)$ of the initial (e.g., the ground) state of the atom at the time of emission, according to

$$E_\nu = -|E_0(\alpha_0)| + \nu\omega \quad (\nu \geq 1) \ . \tag{43}$$

[Recall that in our case one photon ionization, $\nu = 1$, is already possible, see Eq. (9).] The decrease of the ground-state binding energy $|E_0(\alpha_0)|$ with respect to its unperturbed value implies that the whole energy spectrum of the ionized electrons at the time they are *leaving the atom* is shifted towards *higher* energies than in the low intensity case. This is a prediction which can be compared to experiment, if the empirical data are appropriately interpreted (see below). It contrasts with the findings from multiphoton experiments performed in the infrared or the visible at intensities up to 10^{-1} a.u. on noble-gas atoms, e.g., see Refs. 39 and 40. (The fact that the effective potential for the noble-gas atoms is not Coulomb, as in our case, should not play a role in the following.) Under those circumstances an *increase* of the ground-state ionization potential occurs and the lowest-energy ionization peak may be suppressed (see Ref. 41). There is no contradiction with our results, however, since the increase or decrease of $|E_0|$ will depend on ω and I, and our theory does not apply in their case [the frequency condition, Eq. (9), is not satisfied]. Obviously, there can be no suppression of ionization peaks in our regime.

Our formulas for the high-frequency *ionization rates* [see Ref. 3, Eq. (18)] should be calculated from matrix elements having as initial and final states, bound-state eigenfunctions and continuum scattering solutions of Eq. (5), respectively. A calculation of the transition rates according to these formulas is now underway. The extreme atomic distortion (radiative stretching and dichotomy) we have found for the bound states will impose its signature on the features of the ionization. Concerning the angular distributions, interference oscillations are expected to appear due to the peculiar concentration of the electron distribution around the end points $\pm\alpha_0\mathbf{e}$ of the line of nuclear charge; small changes in α_0 in the vicinity of avoided crossings may induce large variations in the cross sections, due to the rapid change in the wave functions. The total decay rates and lifetimes on the other hand will be essential for assessing quantitatively the stability of the atom at high frequencies, a problem which has not been considered before.

The previous comments referred to predictions of our high-frequency theory. We want to discuss now some of its *underlying assumptions* and the extent to which they are fulfilled in experiment.

As all (semiclassical) theories of stationary decay based on the Floquet method,[42] ours too uses a plane-wave description for the radiation field.[43] Obviously, this is an idealized situation, only approximately realized in experiment. What happens in practice is that high intensities can be achieved only in the form of very short laser pulses. Thus the amplitude of the laser pulse acting on the atoms has a space and time variation, and, besides, may vary from shot to shot (in an unknown way). Since the linear extension of the laser pulse, as determined by the focusing lenses, is larger than the wavelength of the light, the variation of the amplitude over the size of each particular atom can be disregarded and, therefore, in this respect plane-wave results are satisfactory.[44] On the other hand, if the time dependence induced by turning on and off the pulse is too rapid, it may well happen that the plane-wave results are not applicable. This difficulty can be avoided if one assumes that the amplitude varies sufficiently slowly ("adiabatically") during: (i) a light period, so that the notion of frequency is still meaningful, (ii) a typical period of the (classical) electronic motion, so that the atom has time to adjust continuously to this variation, without making quantum transitions other than those implied by multiphoton ionization. Under these circumstances our plane-wave results for the eigenvalues and eigenfunctions can still be expected to describe instantaneously the situation, if we replace the constant field amplitude by the slowly varying time function (on the atomic scale) it actually is. To accommodate for the existence of statistics in the photon beam would require a reformulation of the present theory.

It has been pointed out by Lambropoulos[45] that under currently prevailing experimental conditions (infrared to ultraviolet frequencies, nanosecond to picosecond pulses, outer atomic shells) the electrons being ionized may not have the chance to feel the high peak intensities at all, because they will have been ejected from the atom before that. It should be emphasized that the situation is different in the high-frequency regime we are studying, because the ionization is slowed down. In fact we believe that this is the best suited frequency regime to study the effects of high intensities on the atom. In order that this be the case, however, it is not sufficient that condition (9) be satisfied only for the atom in the field at its peak intensity [for which $|E(\alpha_0)|$ may indeed be quite small] but rather for all its intermediate values during the rise of the pulse, so that the atom is not ionized in the process. This implies that, in fact, ω should be large with respect to the unperturbed value of the initial energy $|E_0^m(0)|$, corresponding to $I = 0$. To date there are no intense lasers at frequencies satisfying Eq. (9) for the unperturbed ground state ($|E_0^0(0)| = 1$ Ry), although considerable progress is being made towards achieving high intensities at high frequencies. This is why in order to observe the high-frequency effects predicted here, for the time being one could turn to ionization from excited (Rydberg) initial states of high m. In this case the condition, Eq. (9), can already be quite well satisfied at low intensities ($\alpha_0 \cong 0$) by the frequencies of the existing superintense infrared lasers.

We now return to the practical possibility of observing the high-frequency shift of the energy spectrum of the ionized electrons, see Eq. (43), taking into account the pulsed nature of the laser radiation. In most experiments done in the past, the duration of the pulse was long enough (e.g., several picoseconds or longer) to allow the electron to escape towards the detector while the pulse was still on. Under these conditions the field amplitude a should be considered as a function of $\mathbf{r}$, slowly varying on the atomic scale. The term $e^2a^2(\mathbf{r})/4mc^2$ appearing in Eq. (10) then acts as a "ponderomotive potential" for the escaping electron, and is eventually entirely converted into kinetic energy.[46] In the case of the low-frequency experiments done so far (e.g., Refs. 39 and 40), this kinetic energy has a compensating effect on the increase of the binding energy of the ground state due to the field.[41] The net result is that the *detected* electron energy spectrum is shifted (practically) back to its low intensity position (i.e., as if the $E_0(\alpha_0)$ in Eq. (43) had been equal to that for the unperturbed initial energy). In our high-frequency case, however, the effect of the increase in kinetic energy due to the ponderomotive potential and the decrease of the binding energy of the ground state are additive so that the *detected* electron spectrum should be shifted towards higher energies than predicted by Eq. (43).

On the other hand, more recently, ionization experiments have been carried out with laser pulses short enough (in the 100-fs range[47,48]) that they vanish before the emitted electrons have had the time of leaving them. In this case the energy peaks should indeed be located around the positions predicted by Eq. (43).

ACKNOWLEDGMENTS

We are indebted to Dr. C. W. McCurdy for his collaboration in the early stages of our work. This work was supported by the foundation FOM which is a division of NWO, the Netherlands Organization for Scientific Research.

APPENDIX: GERADE-UNGERADE SPLITTING

For two arbitrary solutions ϕ^S_{mj},ϕ^A_{mj} of the Schrödinger equation, Eq. (5), the following, well-known equation holds (we drop the subscripts m,j for a while):

$$(E^A-E^S)\int_{\bar{V}}\phi^{S*}\phi^A d\mathbf{r} = \tfrac{1}{2}\int_\Sigma[(\nabla\phi^S)^*\phi^A-\phi^{S*}(\nabla\phi^A)]\cdot d\mathbf{S}\ , \tag{A1}$$

where $\bar{V}$ is an integration volume confined by the surface Σ.[49] Allowing $\bar{V}$ to extend over the entire space above the xy plane (i.e., $z>0$), Eq. (A1) can be written as[50]

$$(E^A-E^S)\int_{\bar{V}}\phi^{S*}\phi^A d\mathbf{r}=\tfrac{1}{2}\int_\Sigma\left[\phi^{S*}\frac{\partial\phi^A}{\partial z}\right]dS\ , \tag{A2}$$

where Σ now reduces to the xy plane, as the rest of the confining surface does not contribute. We have taken into account that ϕ^A vanishes in the xy plane.

This equation is exact. We want to apply it now to the limiting case of large α_0. As specific ϕ^S_{mj},ϕ^A_{mj} we would like to use the two forms ϕ^P_{mj} given by Eq. (35) for $P=0$ and 1. This requires some comments. The function u_{mj} is a solution of Eq. (30) containing the endpoint potential Eq. (29). For $r\to\infty$, u_{mj} has the *dominant* behavior

$$u_{mj}(\alpha_0^{-1/3}\mathbf{r}) \underset{r\to\infty}{\sim} \sum_l C_l^{(jm)}Y_{lm}(\theta,\varphi) \times\exp[-(2|W_{|m|j}|)^{1/2}\alpha_0^{-1/3}r]\ , \tag{A3}$$

where the $C_l^{(jm)}$ are constants. Equation (A3) is obtained by neglecting the potential asymptotically in Eq. (30). The xy plane, over which the surface integral of Eq. (A2) should be carried out, is located at a distance α_0 from the end points $\pm\alpha_0\mathbf{e}$. However, at distances of order α_0 (or larger) from both end points, the potential Eq. (29) is a bad approximation to the exact V_0, and one may question if our wave functions Eqs. (35) and (A3) are adequate. That this is nevertheless the case for the purpose of *estimating* to dominant order the value of the surface integral, simply follows from the fact that the exponential in Eq. (A3) can be obtained either from Eq. (5) or from Eq. (30) by completely ignoring the existence of a potential in the area of interest.

For simplicity, we shall introduce in Eq. (35) the notation

$$\begin{aligned} v_{mj}(\mathbf{r})&=\alpha_0^{-1/2}u_{mj}(\alpha_0^{-1/3}\mathbf{r}_-)\ ,\\ v_{mj}(-\mathbf{r})&=\alpha_0^{-1/2}u_{mj}(-\alpha_0^{-1/3}\mathbf{r}_+)\ . \end{aligned} \tag{A4}$$

By inserting the ϕ^S,ϕ^A of Eq. (35) into Eq. (A2), we find

$$\begin{aligned}(E^A-E^S)&\int_{\bar{V}}[v^*(\mathbf{r})\pm v^*(-\mathbf{r})][v(\mathbf{r})\mp v(-\mathbf{r})]d\mathbf{r}\\ &=\frac{1}{2}\int_\Sigma[v^*(\mathbf{r})\pm v^*(-\mathbf{r})]\frac{\partial}{\partial z}[v(\mathbf{r})\mp v(-\mathbf{r})]dS\ ,\end{aligned} \tag{A5}$$

where the upper signs hold for m even and the lower ones for m odd (see Sec. V). Since $v(-\mathbf{r})$ is vanishingly small for $z>0$, and $v(\mathbf{r})$ is normalized to 1, see Eq. (34), the left-hand side of Eq. (A5) is equal to (E^A-E^S). To evaluate the right-hand side of Eq. (A5), we note that v_{mj} of Eq. (A4) has the form of Eq. (42a), see also Eq. (A3).[51] As a consequence, the surface integral in Eq. (A5) has the value

$$4\int_\Sigma v^*(\mathbf{r})\frac{\partial v(\mathbf{r})}{\partial z}dS=2\int_\Sigma\frac{\partial|v(\mathbf{r})|^2}{\partial z}dS \tag{A6}$$

for both m even or odd. Equation (A5) thus becomes

$$E^A-E^S=\int_\infty\int\frac{\partial|v_{mj}|^2}{\partial z}dx\,dy\ . \tag{A7}$$

The large-α_0 behavior of the integral can be obtained by inserting the large-α_0 behavior of v_{mj} from Eqs. (A3) and (A4). We thus end up with the order of magnitude estimate given in Eq. (36).[52]

[*] Present address: Department of Physics, University of Pennsylvania, Philadelphia, PA 19104.

[1] For recent advances see, for example, *Ultrafast Phenomena VI,* edited by T. Yajima, K. Yoshihara, C. B. Harris, and S. Shionoya (Springer, Berlin, 1988), Pts. I and II.

[2] M. Gavrila and J. Z. Kaminski, Phys. Rev. Lett. **52**, 614 (1984).

[3] M. Gavrila, in *Fundamentals of Laser Interactions I,* Vol. 229 of *Lecture Notes in Physics,* edited by F. Ehlotzky (Springer, New York, 1985).

[4] The Coulomb case was treated by M. J. Offerhaus, J. Z. Kaminski, and M. Gavrila, Phys. Lett. **112A**, 151 (1985); J. van de Ree, J. Z. Kaminski, and M. Gavrila, Phys. Rev. A **37**, 4536 (1988); the Yukawa case by M. Gavrila, M. J. Offerhaus, and J. Z. Kaminski, Phys. Lett. A **118**, 331 (1986).

[5] M. Pont and M. Gavrila, Phys. Lett. A **123**, 469 (1987).

[6] M. Pont, N. R. Walet, M. Gavrila, and C. W. McCurdy, Phys. Rev. Lett. **61**, 939 (1988).

[7] M. Pont, M. J. Offerhaus, and M. Gavrila, Z. Phys. **9**, 297 (1988).

[8] A similar behavior was found in the circularly polarized case, see Ref. 7.

[9] H. A. Kramers, *Collected Scientific Papers* (North-Holland, Amsterdam, 1956), p. 866.

[10] W. Pauli and M. Fierz, Nuovo Cimento **15**, 167 (1938).

[11] W. C. Henneberger, Phys. Rev. Lett. **21**, 838 (1968).

[12] The connection between the wave function ψ entering Eq. (2) and the solution ψ_L of the Schrödinger equation in the momentum gauge for the laboratory reference frame is thus $\psi_L(\mathbf{r},t)=\psi(\mathbf{r}-\boldsymbol{\alpha}(t),t)\exp[-(ie^2/2\hbar mc^2)\int_0^t \mathbf{A}^2(t')dt']$.

[13] To second order in the iteration, Eq. (5) is replaced by Eq. (35) of Ref. 3. The correction term in the latter contains $G(\Omega_m)$ the Green's function associated to the Hamiltonian of Eq. (5), taken at values $\Omega_m=E+m\hbar\omega(m\neq 0)$. It is apparent that the correction term becomes as small as desired at sufficiently large ω (with α_0 kept constant).

[14] M. Gavrila and J. Z. Kaminski (unpublished).

[15] The convergence of the high-frequency theory (Refs. 2 and 3) was tested on one-dimensional model atoms with short-range potentials, both for multiphoton ionization and scattering. The case of *ionization* was considered by J. N. Bardsley and M. J. Comella, Phys. Rev. A **39**, 2252 (1989). The Floquet system of coupled equations was solved numerically and compared to the single Floquet-channel calculation based on Eq. (5). The results obtained for the (real part of the) high-frequency eigenvalues agree remarkably well with those predicted by Eq. (5), even at the relatively low photon energies $2.5<\omega/|E_0(\alpha_0)|<5$, where $|E_0(\alpha_0)|$ is the binding energy of the ground state. R. Bhatt, B. Piraux, and K. Burnett, Phys. Rev. A **37**, 98 (1988), considered the case of *scattering* (free-free transitions). Again, by solving numerically the Floquet system, they obtained results for the multiphoton transition amplitudes and compared their magnitude to the elastic amplitude [corresponding to Eq. (5)]. The results indicate the decrease at high frequencies of the former with respect to the latter one [see their Fig. 5(a)], as required by our high-frequency theory.

[16] When the (upgarded) KrF* excimer laser ($\omega=5$ eV) of A. P. Schwarzenbach, T. S. Luk, I. A. McIntyre, U. Johann, A. McPherson, K. Boyer, and C. K. Rhodes, Opt. Lett. **11**, 499 (1986), is operated at intensity $I=1$ a.u. we have $\alpha_0=31$ a.u., and at $I=100$ a.u., $\alpha_0=310$ a.u.

[17] As customary, we have eliminated from the right-hand side of Eq. (10) the rapidly oscillating phase factor $\exp[-(ie^2a^2/8\hbar\omega mc^2)\sin 2\omega t]$.

[18] The "observable" charge density in the laboratory frame should be obtained, as usual, by averaging $|\psi_L(\mathbf{r},t)|^2 = |\psi_0(\mathbf{r}-\boldsymbol{\alpha}(t))|^2$ over a period. Averaged charge densities for the ground state were given for the purpose of illustration in Fig. 2 of Ref. 6.

[19] J. I. Gersten and M. H. Mittleman, J. Phys. B **9**, 2561 (1976).

[20] M. H. Mittleman, *Theory of Laser-atom Interactions* (Plenum, New York, 1982), Chap. 3.

[21] C. K. Choi, W. Henneberger, and F. C. Sanders, Phys. Rev. A **9**, 1985 (1974). References to other work concerning Eq. (5) were given in Ref. 5.

[22] They formulated, however, the validity condition for the *purely plane-wave case* (and for the case of circular polarization they were considering) too restrictively, by requiring that in Eq. (9) ω to be large with respect to the *field-free* ($\alpha_0=0$) value of the ionization potential $|E_0(0)|$, instead of $|E_0(\alpha_0)|$.

[23] The $H_2{}^+$ eigenvalue problem is separable in prolate spheroidal coordinates, a fact which is connected to the conservation of a quantity representing the generalization of the one-center Runge-Lenz vector, see B. R. Judd, *Angular Momentum Theory for Diatomic Molecules* (Academic, New York, 1975), Chap. 4.

[24] L. P. Eisenhart [Phys. Rev. **75**, 29 (1949)] was able to give the forms of all potentials for which the Schrödinger equation, Eq. (5), is separable in *orthogonal* coordinates. None of these may be written as the sum of three or more Coulomb potentials [see C. A. Coulson and A. Joseph, Int. J. Quantum Chem. **1**, 337 (1967)].

[25] J. von Neumann and E. P. Wigner, Z. Phys. **30**, 467 (1929); see also L. D. Landau and E. M. Lifshitz, *Quantum Mechanics, Nonrelativistic Theory* (Pergamon, New York, 1958), Sec. 76.

[26] See, for example, H. Bethe and E. Salpeter, *Quantum Mechanics of One- and Two-Electron Systems* (Springer, Berlin, 1957), Eqs. (39.11)–(39.13); see also C. Frahm, Am. J. Phys. **51**, 826 (1983).

[27] With this prescription the integral of the second term of Eq. (18) multiplied by a spherically symmetric function gives zero.

[28] S. Pasternack and R. M. Sternheimer, J. Math. Phys. **3**, 1280 (1962).

[29] The proof is similar to that given by M. Pont, M. J. Offerhaus, and M. Gavrila, Ref. 7, for the circularly polarized case.

[30] H. Bethe, in *Quantenmechanik der Ein- und Zwei-Elektronenprobleme,* Vol. XXIV/1 of *Handbuch der Physik,* edited by H. Geiger and K. Scheel (Springer, Berlin, 1933), Eqs. (58.8) and (58.9).

[31] A more rigorous proof is planned to be given elsewhere (M. Pont and M. Gavrila, unpublished).

[32] The angular function $K(\sin(\chi/2))$ increases monotonically with χ, from $K=\pi/2$ for $\chi=0$, to infinity when $\chi\rightarrow\pi$. In this limit we have $K\cong\ln[4/\cos(\chi/2)]$; see I. S. Gradshteyn and I. M. Ryzhik, *Table of Integrals, Series and Products* (Academic, New York, 1965), Eq. 8.113.3. The increase is, however, rather slow: at $\chi=160°$, $K=3.35$.

[33] Similar exponential splittings are found in the cases of H_2 and $H_2{}^+$, see Ref. 49. There, however, because of the simpler form of the (Coulomb) potentials involved, also the coefficient in front of the exponential could be determined.

[34] S. Huzinaga, J. Chem. Phys. **42**, 1293 (1965).

[35] S. Huzinaga, Supp. Progr. Theor. Phys. **40**, 52 (1967); I. Shavitt, in *Methods in Computational Physics,* edited by B. Alder, S. Fernbach, and M. Rotenberg (Academic, New York, 1963), Vol. 2, p. 1.

[36] See A. Szabo and N. Ostlund, *Modern Quantum Chemistry*

(Macmillan, New York, 1982), Sec. 3.4.5.

[37] $M(l_i)$ was chosen 3,2.3,2,1.8,1.7,1.7 for $l_i = 0,1,2,3,4,5$, respectively. Thereby, two Gaussians having the same center, which differ only by the factor $M(l_i)$ in their exponents, have an overlap integral of 0.8.

[38] The accuracy of the "decoupled l-channel approximation" calculation of Ref. 5 decreases with increasing α_0. For $\alpha_0 \ll 1$ its results are quite accurate, because a level shift formula identical to Eq. (22) can be derived within the approximation. On the other hand, the large-α_0 behavior it predicts differs from Eqs. (32) and (33). Numerically, for the ground state $(1s)\sigma_g$, the eigenvalues obtained with the approximation differ from the exact ones by 1%, 8%, 17%, and 25% at $\alpha_0 = 1$, 10, 50, and 100, respectively. For the lowest states of the other symmetry types the error can be somewhat smaller (π_g, π_u) or larger (σ_u). For the excited states the relative errors are larger, also due to the occurrence of avoided crossings.

[39] P. Kruit, J. Kimman, H. Muller, and M. van der Wiel, Phys. Rev. A **28**, 248 (1983).

[40] P. Agostini, F. Fabre, and G. Petite, in *Multiphoton Ionization of Atoms,* edited by S. L. Chin and P. Lambropoulos (Academic, New York, 1984), p. 133.

[41] H. Muller and A. Tip, Phys. Rev. A **30**, 3039 (1984).

[42] See, for example, N. L. Manakov, V. D. Ovsiannikov, and L. P. Rapoport, Phys. Rep. **141**, 319 (1986); Shih-I-Chu, Adv. At. Mol. Phys. **21**, 197 (1985).

[43] For the complementary approach of determining the evolution of the electron wave function under the influence of a laser pulse by integration of the time-dependent Schrödinger equation, see K. Kulander, Phys. Rev. A **35**, 445 (1987); **36**, 2726 (1987); **38**, 778 (1988).

[44] Nevertheless, when irradiating an assembly of atoms with the laser pulse, the different atoms, located at various points in it, will feel different intensities.

[45] P. Lambropoulos, Phys. Rev. Lett. **20**, 2141 (1985).

[46] R. R. Freeman, T. J. McIlrath, P. H. Bucksbaum, and M. Bashkansky, Phys. Rev. Lett. **57**, 3156 (1986).

[47] R. R. Freeman, P. H. Bucksbaum, H. Milchberg, S. Darack, D. Schumacher, and M. E. Geusic, Phys. Rev. Lett. **59**, 1092 (1987).

[48] H. G. Muller, H. B. van Linden van den Heuvell, P. Agostini, G. Petite, A. Antonetti, M. Franco, and A. Migus, Phys. Rev. Lett. **60**, 565 (1988).

[49] The idea of using surface integrals [as in Eq. (A1)] to calculate gerade-ungerade splittings orginates with L. P. Gor'kov and L. P. Pitaevskii, Dokl. Akad. Nauk SSSR **151**, 822 (1963) [Sov. Phys.—Doklady **8**, 788 (1964)], who applied it to the case of H_2; see also B. M. Smirnov, Zh. Eksp. Teor. Fiz. **46**, 1017 (1964) [Sov. Phys.—JETP **19**, 692 (1964)], for the case of $H_2{}^+$.

[50] Recall that the vector of the area element $d\mathbf{S}$ in Eq. (A1) points towards the exterior of Σ. This determines the sign in Eq. (A2).

[51] Hence, for $\mathbf{r}$ *in the xy plane* we have $v_{mj}(-\mathbf{r}) = (-1)^m v_{mj}(\mathbf{r})$, $[\partial v_{mj}(-\mathbf{r})/\partial z] = (-1)^{m+1}[\partial v_{mj}(\mathbf{r})/\partial z]$.

[52] Upon inserting only the exponential of Eq. (A3) into Eq. (A7), the integral can be calculated using (plane) polar coordinates, by elementary methods. This yields the dominant, large-α_0 behavior given by Eq. (36). The presence of the θ-dependent prefactor in Eq. (A3) (the φ dependence cancels out when taking $|v|^2$) will not change the dominant behavior, and was accounted for by introducing the slowly varying function $A_{|m|j}(\alpha_0)$ in Eq. (36).